Detection Capability Evaluation of Lunar Mineralogical Spectrometer: Results from Ground Experimental Data

Fang Gao[1,2,3], Bin Liu[1,2], Xin Ren[1,2], Da-Wei Liu[1,2], and Chun-Lai Li[1,2]

[1] Key Laboratory of Lunar and Deep Space Exploration, Chinese Academy of Sciences, Beijing 100101, China; liub@nao.cas.cn
[2] National Astronomical Observatories, Chinese Academy of Sciences, Beijing 100101, China
[3] University of Chinese Academy of Sciences, Beijing 100049, China

Abstract

The Chang'E-6 mission will first land on the far side of the moon and bring lunar samples back. As a hyperspectral imager aboard the Chang'E-6 lander, the Lunar Mineralogical Spectrometer (LMS), will achieve the goal of spectral detection and mineral composition analysis in the sampling area, and the data of LMS will also be compared with the results of the returned sample laboratory measurements. Visible and near-infrared hyperspectral remote sensing is an effective tool for lunar minerals identification and quantification. The ground validation experiment can be used to evaluate the detection ability of the LMS. According to the modal abundances of lunar minerals and glasses of APOLLO samples, binary mixed samples, ternary mixed samples, and seven-membered mixed samples were prepared. The samples were ground and stirred homogeneous to about 200 mesh (median particle size about 75 μm), to simulate the soil state of the lunar surface. Under the laboratory ambient condition, the 480–3200 nm spectral data of the samples were acquired using the Engineering Qualification Model (EQM) of Chang'E-5 LMS, the performance of which is consistent with the flight model of Chang'E-6 LMS. By fitting the mixed samples' spectral data of the EQM using the Modified Gaussian Methods, the following conclusions can be drawn: The subtle spectral changes of mixed samples can be detected. The modal abundance of low-Ca pyroxene, high-Ca pyroxene, and plagioclase can be derived based on the spectral parameters such as absorption position, depth or width of the mixed samples, and the correlation coefficients R^2 are better than 82%, indicating that the LMS has good quantitative detection capability.

Key words: methods: data analysis – techniques: spectroscopic – Moon

1. Introduction

With the successful implementation of the Chang'E-5 mission, the Chang'E-6 probe will be launched in 2024. The Chang'E-6 mission will achieve the goal of first landing and samples return on the farside of the Moon. As one of the scientific payloads of Chang'E-6 probe, the Lunar Mineralogical Spectrometer (LMS) will be responsible for the visible and near-infrared spectral detection of the landing area, mineral types, and their distribution survey. Besides, the data of LMS will also be compared with the sample laboratory measurement results.

The composition and distribution of the materials on the lunar surface are important to study the origin and evolution of the moon (Pieters et al. 1993; Williams et al. 1995; Tompkins & Pieters 1999; Jolliff et al. 2000; Elkins Tanton et al. 2002; Cahill et al. 2009; Karthi et al. 2022; Wang et al. 2022). It has been a very effective tool to use visible and near-infrared spectroscopy technology to derive the surface material composition and distribution. It can not only obtain the content and distribution of some useful elements, such as Fe, Ti, Mg, and Al (Lucey et al. 1998, 2000; Ling et al. 2011a, 2011b;

Wu et al. 2012; Yan et al. 2012; Lu et al. 2021) but also the content and distribution of some composed minerals, such as pyroxene, plagioclase, olivine and ilmenite (sunshine & Pieters 1993; Pieters 2002; Shkuratov 2003; Shuai et al. 2013). However, there are still many uncertainties in the identification and quantification of the minerals on lunar surface. For example, the detection and identification of olivine will be mainly influenced by the spectral characteristics of pyroxene in the lunar soil (Singer 1981; Cloutis et al. 1986; De León et al. 2006). Besides, Mg-olivine (forsterite) and Fa-olivine (fayalite) have quite different spectra with different peak positions of three major bands, so they can be clearly distinguished. But when we are talking about the high-resolution distinction of Mg#, it may be highly uncertain (Clark et al. 2007).

To ensure that the payload can work properly and return high-quality scientific data, the LMS needs to calibrate and go through the ground validation experiment before launching. The spectral quality of the LMS has been evaluated in previous investigations (Cai et al. 2019). In this paper, binary mixed samples, ternary mixed samples, and seven-component
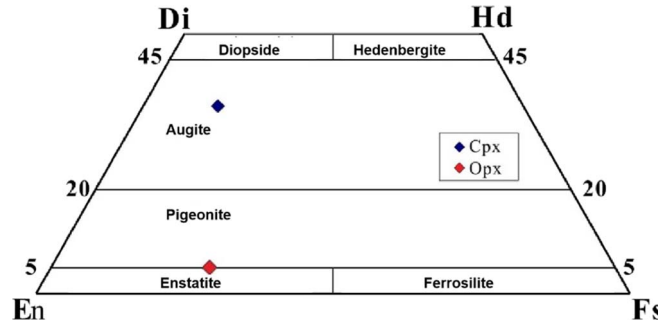
Figure 1. The mineral composition of the two pyroxenes.

Table 1
The Main Characters of LMS

Number	Parameters	Results			
		VIS	NIR	SWIR	MWIR
1	Spectral range (nm)	450 $\sim$ 950	900 $\sim$ 1450	1400 $\sim$ 2300	2200 $\sim$ 3200
2	Spectral resolution (nm)	2 $\sim$ 10	3 $\sim$ 12	8 $\sim$ 24	10 $\sim$ 25
3	Field of view (°)	4.17 $\sim$ 4.17			
6	S/N (dB)	Peak 55, minimum 34			
7	MTF	>0.1			
8	Detect distance (m)	2 $\sim$ 5			

Table 2
Modal Abundance of Different Mineral Samples in Simulated Glass Preparation

Samples	Modal Abundance of Different Minerals (wt%)					
	Hypersthene	Olivine	Plagioclase	Ilmenite	Apatite	Augite
Simulated glass	21.2	8.23	35.66	5.24	8.47	21.2

mixed samples were prepared respectively according to the distribution characteristics of typical mineral components on the lunar surface. By measuring the samples' spectra and fitting the data using the Modified Gaussian Model (MGM), the minerals' quantification capabilities of LMS were analyzed.

2. Instrument Overview

LMS is composed of a two-dimensional scanning motor and a spectrometer (Liu et al. 2022). The spectrometer consists of a Visible and near-infrared imaging detector (VIS, 480–950 nm) and three infrared single-point detectors (NIR, 900–1450 nm; SWIR, 1400–2300 nm; MWIR, 2200–3200 nm). The main characteristics of LMS are listed in Table 1.

LMS carries a calibration target to perform in situ radiometric calibration. The calibration target is embedded in the inner side of the dust cover. When the lander lands on the Moon, the dust cover is opened and fixed at an angle of 70°, then the calibration target is exposed to the sunlight at that angle. LMS detects the landing area by adjusting the observation angle using the two-dimensional pointing mechanism, and also achieves the field of view alignment with the calibration target, to complete in situ radiometric calibration.

3. Laboratory Spectral Measurements

3.1. Experimental Samples

According to the typical minerals and glasses of the lunar surface, six mineral samples and one simulated glass sample were prepared, the mineral samples included clinopyroxene
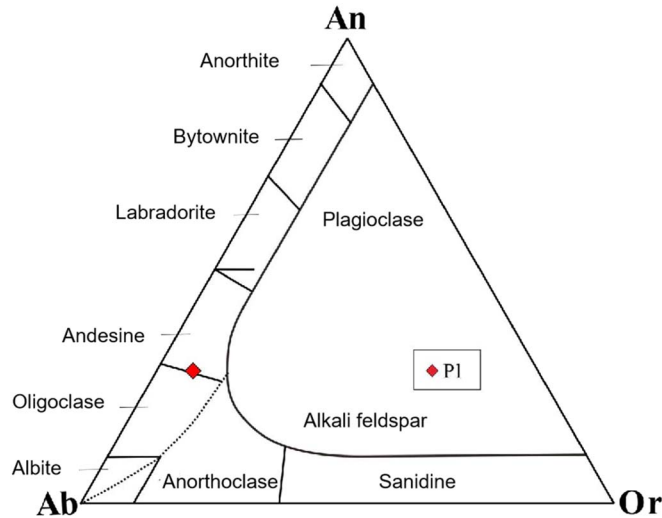
Figure 2. The mineral composition of the plagioclase.
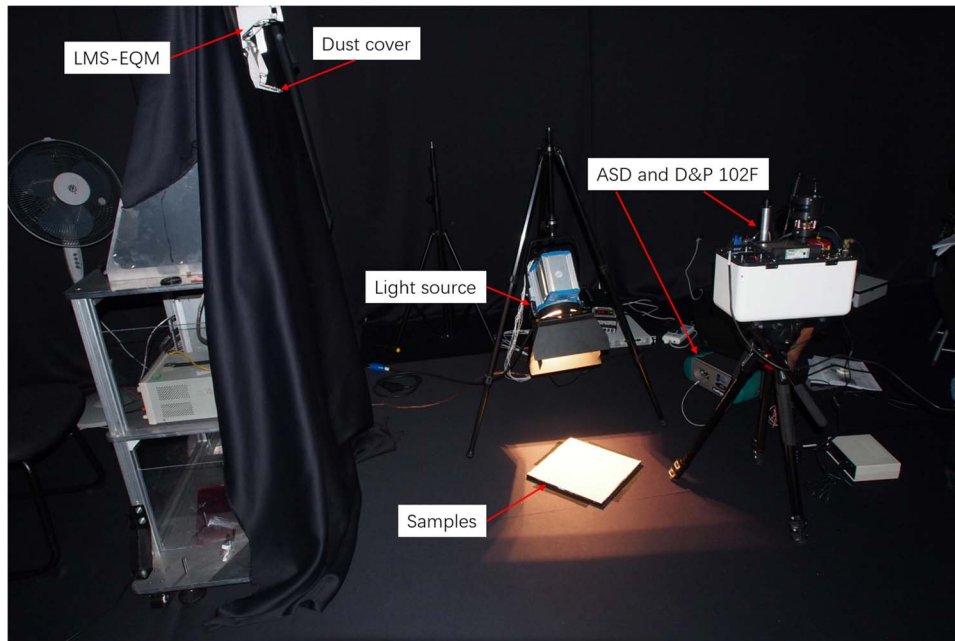
Figure 3. The experimental environment. The "solar-like" lamp can adjust the incident angle of light, and the sample in the container is smoothed and covers the LMS' field of view. The EQM of LMS is fixed to the simulated lander on the left side, the standard spectrometers (ASD and DP102F) are mounted to the simulated lander on the right side, which is mounted in a symmetrical position to the EQM of LMS.

(augite), Orthopyroxene (hypersthene), olivine, ilmenite, apatite, and plagioclase. All mineral samples (except plagioclase) are ground to 200 mesh (about 75 μm), which is similar to the median particle size of lunar soil (40–130 μm). Pure plagioclase samples are obtained by crushing and grounding gabbro to 40 mesh ($\sim$420 μm) first and then removing the magnetic minerals with a magnetic separator. The simulated glass

samples are prepared as follows: different mineral samples were mixed first according to the modal abundances in Table 2, and then the mixed samples were sintered at high temperature (1150°, three hours), quenched, and then ground to 200 mesh to obtain simulated glass samples.

All mineral and glass samples have been analyzed for chemical composition using the sequential X-ray fluorescence

Table 3
Results of Chemical Composition Analysis of the Mineral Samples

Samples	SiO$_2$	TiO$_2$	Al$_2$O$_3$	Cr$_2$O$_3$	NiO	MnO	MgO	CaO	Na$_2$O	K$_2$O
Augite	46.14	1.02	9.71	0.0112	0.0389	0.126	15.81	16.43	2.00	0.0100
Hypersthene	47.59	0.868	6.13	0.0970	0.0195	0.254	24.48	2.45	0.567	0.0923
Olivine	1.10	⋯	0.143	⋯	⋯	0.0292	0.0392	60.28	0.164	⋯
Plagioclase	57.06	0.0577	24.6	⋯	⋯	0.0302	0.541	5.91	7.54	⋯
Ilmenite	10.38	43.78	3.69	0.0471	⋯	1.54	1.07	0.364	⋯	0.124
Simulated glass	44.21	2.58	11.45	0.0265	0.0489	0.190	16.75	9.93	2.83	0.471
Apatite	0.797	⋯	0.271	⋯	⋯	0.0711	0.349	58.48	0.237	0.0087

Table 4
The Experimental Purpose and the Mixture Samples Used

Types of Mixed Samples	Sample Description	Experimental Purpose
binary mixed samples	Composed of augite and hypersthene. The modal abundances of minerals are shown in Table 5.	Changing the proportions of high-calcium pyroxenes and low-calcium pyroxenes, to evaluate whether LMS can detect the subtle spectral changes and whether the modal abundances of the two pyroxenes can be quantified.
ternary mixed samples	Composed of hypersthene, olivine, and plagioclase. The modal abundances of minerals are shown in Table 6.	Changing the proportions of plagioclase and studying the effect on spectral characteristics to evaluate whether LMS can detect subtle spectral changes and whether the modal abundance of plagioclase can be quantified.
seven-membered mixed samples	Composed of augite, hypersthene, olivine, plagioclase, ilmenite, simulated glasses, and apatite. The modal abundances of minerals and glass are shown in Table 7.	Changing the modal abundances of minerals as that of the APOLLO samples, to study the spectral changes of the mixture, and to evaluate the detection ability of LMS and minerals identification and quantification.
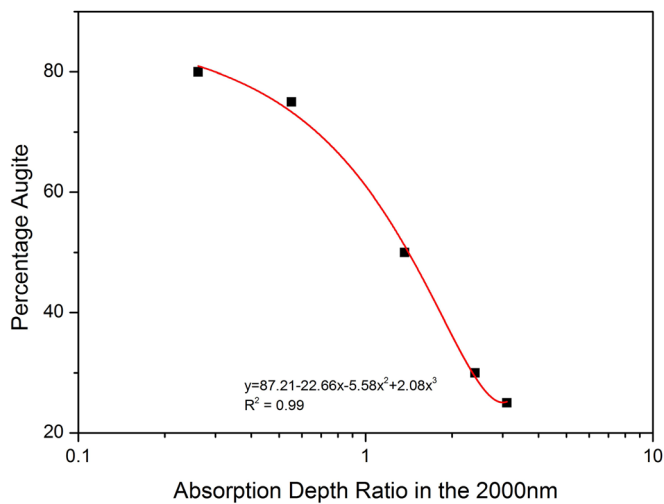
Figure 4. The fitted model for the modal abundances of augite in the binary mixed samples.

spectrometer, and the results are shown in Table 3 and Figures 1 and 2. To simulate the mineral composition of the lunar soils, binary mixed samples, ternary mixed samples, and seven-members mixed samples were prepared. The sample description and experimental purpose are shown in Tables 4–7. The spectra of all the minerals and mixed samples in the 480–3200 nm were measured and displayed in our previous paper (Cai et al. 2019).

3.2. Experimental Environment and Process

The experiment is implemented in a dark room, and the environment is shown in Figure 3. The spectral data acquisition of seven mineral samples and 18 mixed samples were completed sequentially using the Engineering Qualification Model (EQM) of LMS and the standard spectrometers (ASD and DP102F). The full spectral data of the calibration targets (an aluminum panel and a gold panel) were also acquired at the
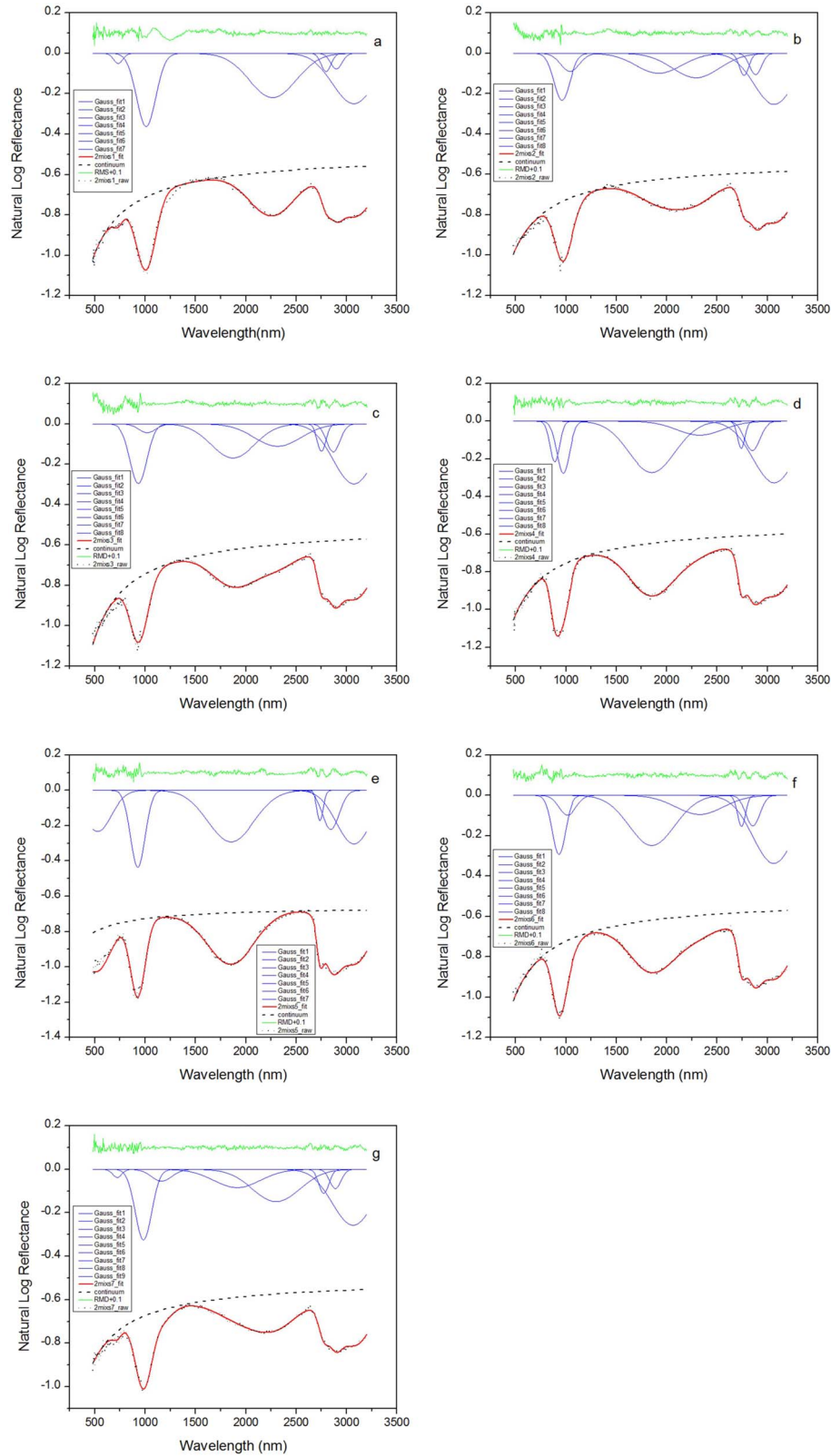
Figure 5. The MGM fitting results of the binary mixed samples' spectra obtained by the EQM of LMS.
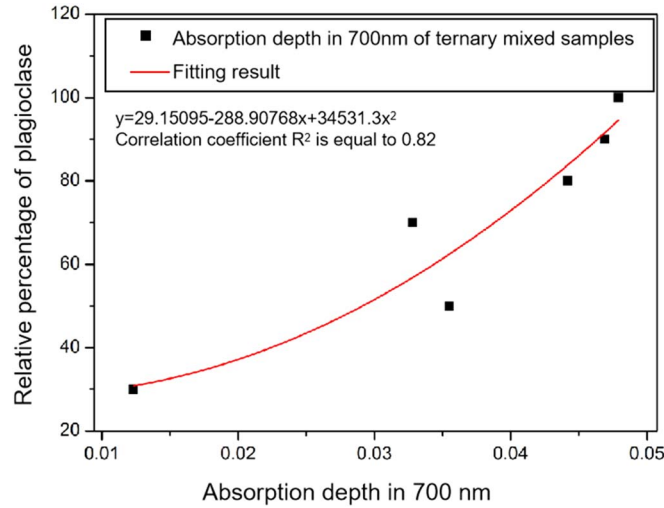
Figure 6. The fitted model for the modal abundances of plagioclase in the ternary mixed samples.

Table 5
The Mineral Composition of Binary Mixed Samples (sunshine & Pieters 1993)

Types of Mixed Samples	The Mineral Composition (wt%)	
	Hypersthene	Augite
Sample 1	0	100
Sample 2	25	75
Sample 3	50	50
Sample 4	75	25
Sample 5	100	0
Sample 6	70	30
Sample 7	20	80

Table 6
The Mineral Composition of Ternary Mixed Samples (Serventi et al. 2013)

Types of Mixed Samples	The Mineral Composition (wt%)		
	Hypersthene	Olivine	Plagioclase
Sample 1	70	30	0
Sample 2	49	21	30
Sample 3	35	15	50
Sample 4	21	9	70
Sample 5	14	6	80
Sample 6	7	3	90
Sample 7	0	0	100

same time. After reflectance data calculation, the spectral parameters of absorption centers, depths, and widths are also derived.

4. Detection Capability Evaluation

4.1. Detection Capability Evaluation of the Binary Mixed Samples

Binary mixed samples were prepared by mixing augite and hypersthene in different proportions (Table 5). We acquired spectra of binary mixed samples, analyzed the subtle spectral changes with mineral contents, and evaluated the ability of LMS to quantify the composed minerals.

With the composition of the binary mixed samples changed, the absorption centers and depths of the samples changed regularly. The MGM is used to fit the spectra and the functional relationship can be found between the modal abundance of augite and the absorption depth ratio in the 2000 nm, which is defined as the absorption strength of

hyperthene component divided by the absorption strength of augite component. The fitting result shows that with the increase of the modal abundance of augite, the absorption depth ratio of augite in the 2000 nm decreases gradually (Figure 4), and the polynomial fitting coefficient R^2 is equal to 0.99. Figure 5 demonstrates the MGM results of the binary mixed samples. As shown in Figure 5, the hydration bands near 3 μm are fitted by three Gaussians to beyond the data noise level (Hiroi et al. 2021).

4.2. Detection Capability Evaluation of the Ternary Mixed Samples

The ternary mixed samples were prepared by mixing hypersthene, olivine, and plagioclase, in which the ratio of hypersthene to olivine remained unchanged, but the content of plagioclase is changed. We acquired spectra of the ternary mixed samples, analyzed the spectral changes, and evaluated the detection capability of LMS for plagioclase quantification.
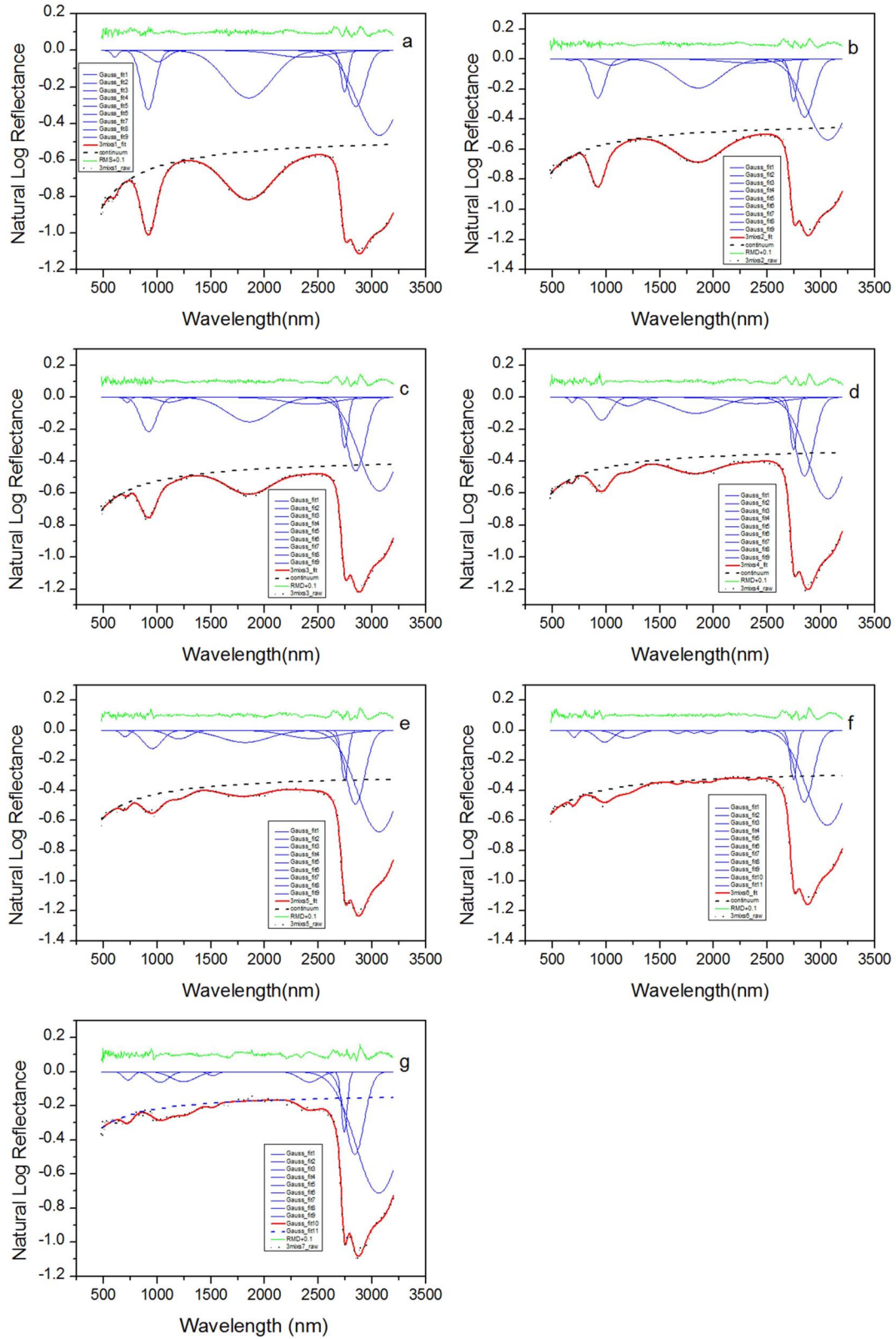
Figure 7. The MGM results of the ternary mixed samples' spectra obtained by the EQM of LMS.
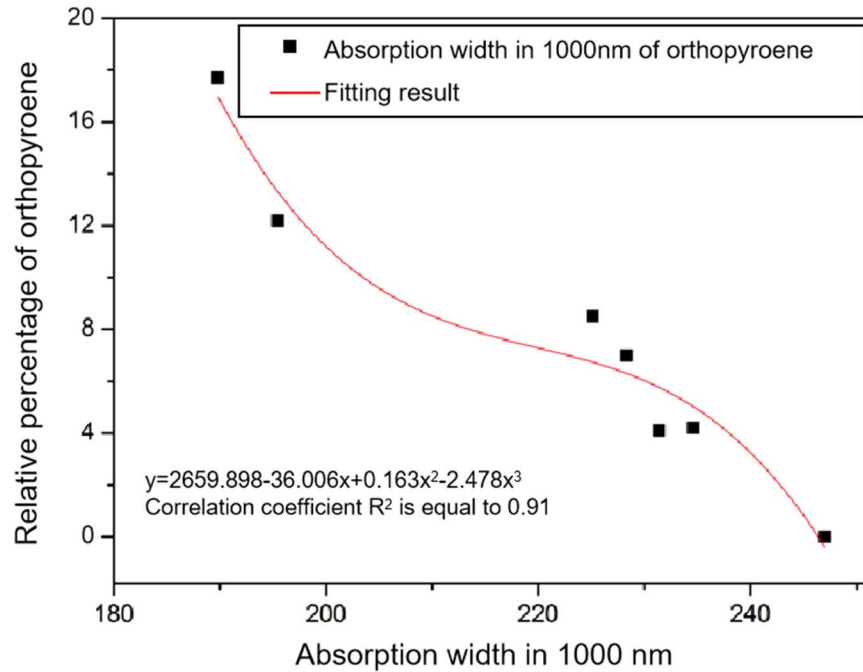
Figure 8. The fitted model for the modal abundances of the orthopyroxene in the seven-membered mixed samples.

Table 7
The Minerals and Glass Composition of the Seven-membered Mixed Samples

Types of Samples	The Minerals and Glass Composition (wt%)						
	Hypyerthene	Olivine	Plagioclass	Ilmenite	Apatite	Simulated Glass	Augite
Sample 1	12.2	1.2	17.1	5.5	2.9	61.1	0.0
Sample 2	17.7	3.5	15.8	2.9	4.8	49.4	5.9
Sample 3	8.5	3.3	14.3	2.1	3.4	59.9	8.5
Sample 4	4.2	2.9	19.0	1.7	3.7	56.1	12.4
Sample 5	0.0	2.1	16.6	0.8	3.8	61.8	14.9
Sample 6	4.1	4.1	15.7	9.3	1.0	56.0	9.8
Sample 7	7.0	3.6	17.2	6.2	0.8	63.5	1.7

Note. Reference: the mass percentage of minerals in APOLLO returned samples.

With the increasing of the plagioclase content, the amplitudes of reflectance are getting higher, and the plagioclase absorption peak depth near 700 nm, which is defined as the strength of the Gaussian around 700 nm fitted by the MGM, are much more obvious, but the absorptions of pyroxene near 1000 and 2000 nm are gradually weakened. The MGM is used to fit the spectra and the functional relationship is established between the modal abundance of plagioclase and the absorption depth in the 700 nm. The fitting result shows that the higher the plagioclase content, the deeper the absorption peak depth in the 700 nm (Figure 6), and the polynomial fitting

coefficient R^2 is equal to 0.82. Figure 7 shows the MGM results of the ternary mixed samples.

4.3. Detection Capability Evaluation of the Seven-members Mixed Sample

The seven-members mixed samples are mixtures of augite, hypersthene, olivine, plagioclase, ilmenite, apatite, and simulated glass according to the contents of minerals in the APOLLO lunar soil samples. We acquire spectra of the seven-members mixed samples and analyze the relationship between the variation of the spectral characteristics with the content of
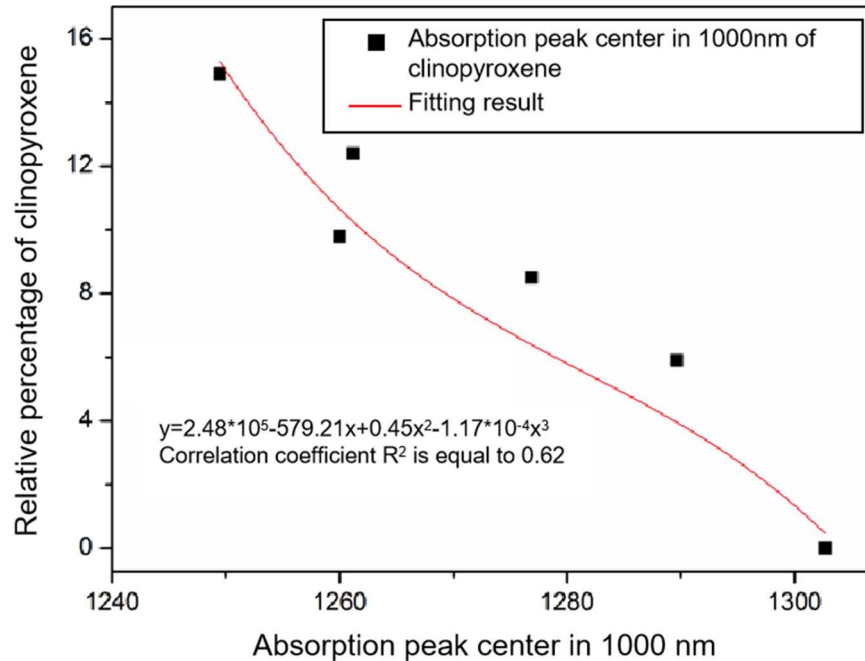
Figure 9. The fitted model for the modal abundances of clinopyroxene in the seven-membered mixed samples.

each mineral, to evaluate the ability of LMS for various minerals quantification.

With the change in the mineral contents, the characteristics of absorptions and the reflectance amplitude of the seven-membered mixed samples were both changed. The MGM is also used to fit the spectra and the functional relationship is established between the absorption width of the hypersthene in 1000 nm and the modal abundances of the hypersthene, and the functional relationship is also established between and the absorption positions of augite in 1000 nm and the modal abundance of the augite. The fitting results are shown in the following Figures 8 and 9. The correlation coefficients are $R^2 = 0.91$ and $R^2 = 0.62$. We also try to find the relationships between the modal abundances of other kinds of minerals in the seven-membered mixed sample and the MGM spectral parameters, but no good fitting results are found. Figure 10 shows the MGM fitting results of the seven-membered mixed samples.

5. Conclusion and Discussion

5.1. Conclusion

The ground validation experiment is conducted in the laboratory for the EQM of LMS, spectral data acquisition, and MGM modeling were performed on the binary mixed samples, ternary mixed samples and the seven-members mixed samples. It can be concluded that LMS can effectively detect the subtle spectral variations in the mixed samples. The quantification model of the binary mixed samples can correctly reflect the relationship between the modal abundance of augite

and the absorption depth ratio in 2000 nm, with the correlation coefficient $R^2 = 0.99$. The quantification model of the ternary mixed samples can also properly reflect the relationship between the modal abundances of plagioclase and the absorption band depths in 700 nm, with the correlation coefficient $R^2 = 0.82$. In addition, The quantification models of the augite and the hyperthene in the seven-members mixed samples are also established, with the correlation coefficients $R^2 = 0.91$ and $R^2 = 0.62$. The results demonstrate that LMS has good spectral identification and quantification ability.

5.2. Discussion

The quantification models for plagioclase, olivine, ilmenite, simulated glass, and apatite were not built in the seven-members mixed samples. The possible reasons are as follows: First, MGM allows spectra to be analyzed directly, without using end-member spectra. But this model could only quantify modal abundances of minerals with absorption features. Apatite, with a very low content, has no obvious absorption features except for the structural water's absorption near 2.7 μm, so it is difficult to be identified and quantification. Besides, the low content of olivine in the seven-members mixed samples makes that it cannot be quantified from the mixture spectra, although it has obvious absorption features near 1 m. The characteristic of the low albedo and low contents of Ilmenite in the mixed samples also make it hard to identify and quantify. In addition, although plagioclase and simulated glass have relatively high modal abundances, their contents vary in a narrow range, so the
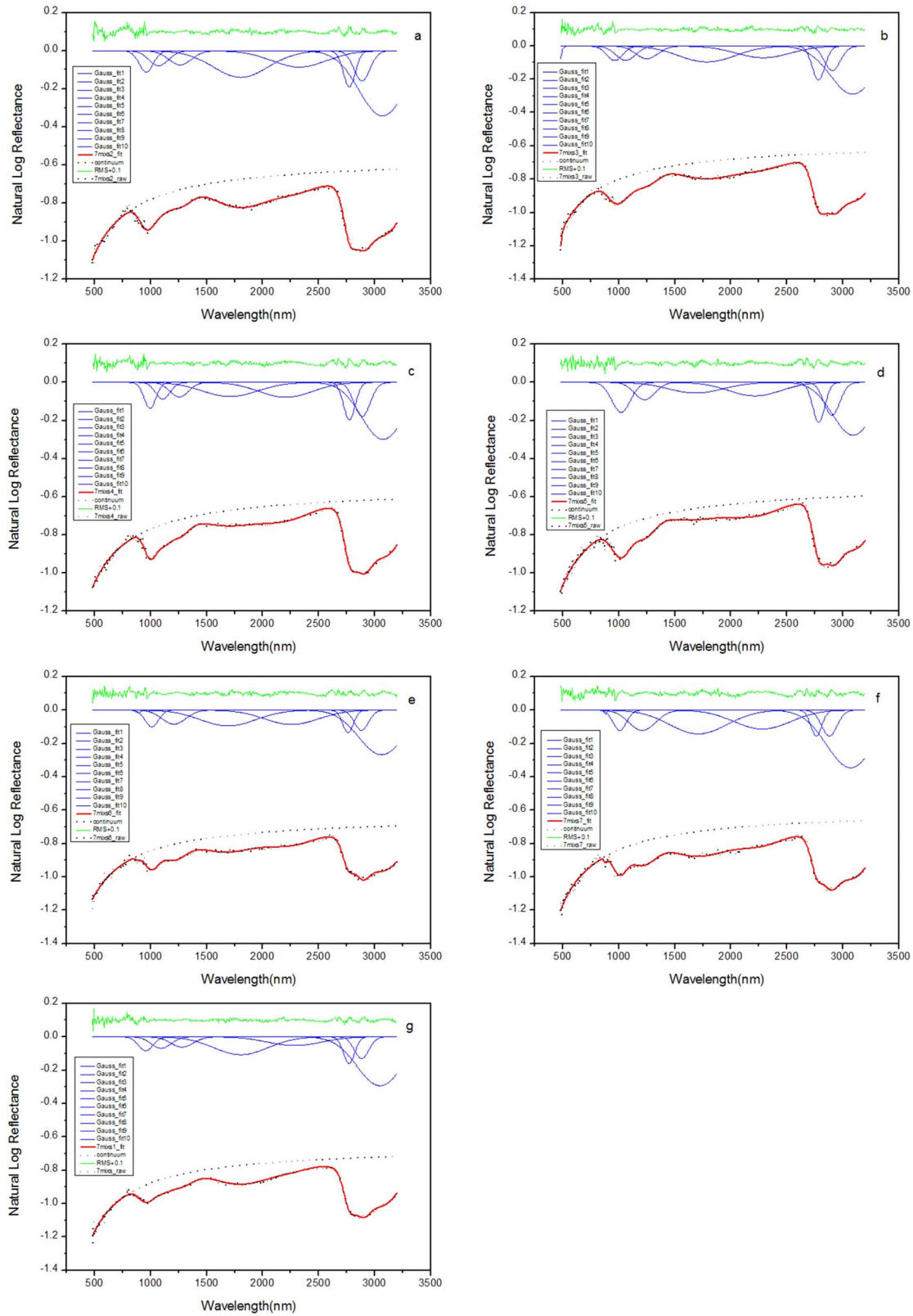
Figure 10. The MGM fitting results of the seven-membered mixed samples obtained by the EQM of LMS.

spectral variations are still not obvious. For example, the modal abundance of plagioclase only varies from 14.3% to 17.2%. Previous studies by Pieters et al. (2014) indicate that the absorption features of plagioclase are suppressed by that of pyroxene when plagioclase is mixed with pyroxene. The plagioclase can be only identified and quantified when the contents of plagioclase in the mixture reach above 80%.

References

Cahill, J. T. S., Lucey, P. G., & Wieczorek, M. A. 2009, JGRE, 114, E09001
Cai, T.-n., Li, C.-l., He, Z.-p., et al. 2019, Spectrosc. Spectral Anal., 39, 257
Clark, R. N., Swayze, G. A., Wise, R. A., et al. 2007, USGS Digital Spectral Library Splib06a, Report, 231
Cloutis, E. A., Gaffey, M. J., Jackowski, T. L., & Reed, K. L. 1986, JGR, 91, 11641
De León, J., Licandro, J., Duffard, R., & Serra-Ricart, M. 2006, AdSpR, 37, 178
Elkins Tanton, L. T., Van Orman, J. A., Hager, B. H., & Grove, T. L. 2002, E&PSL, 196, 239
Hiroi, T., Kaiden, H., Imae, N., et al. 2021, PolSc, 29, 100723
Jolliff, B. L., Gillis, J. J., Haskin, L. A., Korotev, R. L., & Wieczorek, M. A. 2000, JGRE, 105, 4197
Karthi, A., Arivazhagan, S., & Sharma, M. 2022, RAA, 22, 125002
Ling, Z., Zhang, J., Liu, J., et al. 2011a, ChSBu, 56, 376
Ling, Z., Zhang, J., Liu, J., et al. 2011b, ChSBu, 56, 2082
Liu, J., Liu, B., Ren, X., et al. 2022, NatCo, 13, 3119
Lu, Y., Wu, Y.-Z., Li, C., et al. 2021, RAA, 21, 031
Lucey, P. G., Blewett, D. T., & Hawke, B. R. 1998, JGRE, 103, 3679
Lucey, P. G., Blewett, D. T., & Jolliff, B. L. 2000, JGRE, 105, 20297
Pieters, C. 2002, Icar, 155, 285
Pieters, C. M., Head, J. W., Sunshine, J. M., et al. 1993, JGR, 98, 17127
Pieters, C. M., Murchie, S., Thomas, N., & Britt, D. 2014, P&SS, 102, 144
Serventi, G., Carli, C., Sgavetti, M., et al. 2013, Icar, 226, 282
Shkuratov, Y. G. 2003, JGR, 108, 5020
Shuai, T., Zhang, X., Zhang, L., & Wang, J. 2013, Icar, 222, 401
Singer, R. B. 1981, JGRB, 86, 7967
Sunshine, J. M., & Pieters, C. M. 1993, JGRE, 98, 9075
Tompkins, S., & Pieters, C. M. 1999, M&PS, 34, 25
Wang, R.-G., Su, Y., Zhang, Z.-Y., et al. 2022, RAA, 22, 105002
Williams, D. A., Greeley, R., Neukum, G., Wagner, R., & Kadel, S. D. 1995, JGR, 100, 23291
Wu, Y., Xue, B., Zhao, B., et al. 2012, JGRE, 117, E02001
Yan, B., Xiong, S. Q., Wu, Y., et al. 2012, P&SS, 67, 119